Quantum Hard Spheres with Affine Quantization

Riccardo Fantoni*
Università di Trieste, Dipartimento di Fisica, strada Costiera 11, 34151 Grignano (Trieste), Italy
(Dated: November 24, 2025)

We study a fluid of quantum hard-spheres treated with affine-quantization. Assuming that the fluid obeys to Bose-Einstein statistics we solve for its thermodynamic properties using the path integral Monte Carlo method.

Keywords: Hard-Spheres; Affine-Quantization; Bose-Einstein Statistics; Path Integral Monte Carlo; Thermodynamics

I. INTRODUCTION

The simplest model of a fluid [1] is a system of hard spheres, for which the pair potential $\Phi_{\rm HS}(r)$ at a separation r is

$$\Phi_{\rm HS}(r) = \begin{cases} +\infty & r < \sigma \\ 0 & \text{else} \end{cases}, \tag{1.1}$$

where σ is the hard-sphere diameter. This simple potential is ideally suited to the study of phenomena in which the hard core of the potential is the dominant factor. Much of our understanding of the properties of the hard-sphere model come from computer simulations [2, 3]. Such calculations have revealed very clearly that the structure of a hard-sphere fluid does not differ in any significant way from that corresponding to more complicated interatomic potentials, at least under conditions close to crystallisation.

The most important feature of the pair potential of a liquid is the strong repulsion that appears at short range and is due to the overlap of the outer electron shells inhibited by the Pauli exclusion principle. This strongly repulsive forces are responsible for the short range order characteristic of the liquid state. The attractive forces acting at long range are much more smooth and play only a minor role in determining the structure of the liquid. They provide an almost uniform attractive background giving rise to the cohesive energy that stabilizes the liquid.

However, although simulations show that the hard-sphere *classical* fluid undergoes a freezing transition at a reduced number density $\rho^\star = \rho\sigma^3 \approx 0.945$ [2, 4], the absence of attractive forces means that there is only one fluid phase. The properties of hard-spheres are better understood in terms of the so called packing fraction $\eta = \rho v_d \sigma^d$ where

$$v_d = \frac{(\pi/4)^{d/2}}{\Gamma(1+d/2)}, \tag{1.2}$$

is the volume of a d-dimensional sphere of unit diameter (for instance $v_3 = \pi/6$, so that $0 < \eta < v_3\sqrt{2}$ since one cannot pack spheres more than their closest packing configuration in three dimensions).

The hard-sphere fluid is also considered as the reference system for a pair potential perturbation theory [1, 5–7].

Least but not least the classical hard-sphere fluid admits exact analytic solution for the Percus-Yevick integral equation theory through the Wiener-Hopf factorization [8–13]

Now the *quantum* version of the hard-sphere fluid has seldomly been treated. This can be explained by the difficulties that one faces when treating hard-walls in quantum mechanics [14]. In order to overcome the difficulty of having to deal with a canonical momentum that is not anymore a self-adjoint operator a possible way out strategy is to use *affine quantization* instead of the usual Dirac canonical quantization [15].

In this work we will define the model of Quantum Hard-Spheres treated with Affine Quantization (AQHS) and then we will carry out some Path Integral Monte Carlo (PIMC) simulations for a canonical ensemble of the fluid of AQHS in thermal equilibrium at finite non-zero temperature.

* riccardo.fantoni@scuola.istruzione.it

II. THE MODEL

The Hamiltonian for a d-dimensional system of N Bose (BHS) Quantum (QHS) Hard-Spheres (HS) treated with Affine-Quantization (AQ) is as follows [16]

$$H = \lambda \sum_{i=1}^{N} \frac{\partial^2}{\partial \boldsymbol{r}_i^2} + \sum_{i<j} \phi_{\rm AQ}(r_{ij}) + \sum_{i<j} \phi_{\rm HS}(r_{ij}), \tag{2.1}$$

where σ is the diameter of the spheres of mass m, $\lambda = \hbar^2/2m$, $\boldsymbol{r}_i$ is the position of the ith sphere center, $\boldsymbol{r}_{ij} = \boldsymbol{r}_i - \boldsymbol{r}_j$, the HS pair potential $\phi_{\rm HS}(r)$ of Eq. (1.1), and the AQ effective pair potential

$$\phi_{\rm AQ}(r) = \hbar^2 \frac{2r^2 + \sigma^2}{(r^2 - \sigma^2)^2}. \tag{2.2}$$

The latter has a repulsive spike at contact $r = \sigma$. So that the QHS repel each other before getting into (classical) contact. And at large r, $\phi(r) \approx a^2/r^2$, with $a = \hbar\sqrt{2}$, which has a long range repulsive character in $d > 1$. So, in order for the system to admit a thermodynamic limit one needs to add a uniform background with the effect to modify the AQ pair potential as follows

$$\phi_{\rm AQ}(r) \to \phi_{\rm AQ}(r) - \frac{N}{N-1} D_d, \tag{2.3}$$

$$D_d = \frac{1}{\Omega} \int_{\Omega, r>\sigma} \phi_{\rm AQ}(r)\, d\boldsymbol{r} \approx \begin{cases} 24(L-\sigma)/L^3 & d = 3 \\ 16 \ln(L/\sigma)/L^2 & d = 2 \end{cases} \tag{2.4}$$

where $\Omega = L^d$ is the volume of the cubic box (approximated to a sphere of radius $L/2$ in Eq. (2.4) containing the system of QHS in thermal equilibrium at an inverse temperature $\beta = 1/k_B T$ with k_B the Boltzmann constant and T the absolute temperature. This procedure is justified by requiring that the total potential energy $\widehat{V} = \int d\boldsymbol{r} d\boldsymbol{r}'\, \rho(\boldsymbol{r})\rho(\boldsymbol{r}')\phi_{\rm AQ}(|\boldsymbol{r} - \boldsymbol{r}'|)$ remains unchanged under the transformation (2.3) keeping the local number density $\rho(\boldsymbol{r}) = \sum_i \delta^d(\boldsymbol{r} - \boldsymbol{r}_i)$, where δ^d is the d-dimensional Dirac delta function, or under the transformation $\rho(\boldsymbol{r}) \to \rho(\boldsymbol{r}) + \rho_b$, where $\rho_b = -\rho = -N/\Omega$ is the uniform background density, keeping the pair potential $\phi_{\rm AQ}(\boldsymbol{r})$ constant.

III. THE PATH INTEGRAL MONTE CARLO METHOD

The basis for our quantum simulation is imaginary time path integral [17]. We will treat the N AQHS as bosons interacting with the Hamiltonian of Eq. (2.1). Then the quantum statistical mechanics problem reduces to use path integral [18] to calculate the thermal *density matrix* elements $\langle R|e^{-\beta H}|R'\rangle$ as the following path average

$$\langle R|e^{-\beta H}|R'\rangle = \int dR_1 \int dR_2 \cdots \int dR_{M-1}\, e^{-S(R_0, R_1, R_2, \ldots, R_M)}, \tag{3.1}$$

where $R_i = (\boldsymbol{r}_{1,i}, \boldsymbol{r}_{2,i}, \ldots, \boldsymbol{r}_{N,i})$ for $i = 1, 2, \ldots, M$ are the "beads" attached to the M timeslices that form the "polymer" of the Feynman "classical-quantum" isomorphism [19]. And $R_0 = R = (\boldsymbol{r}_1, \boldsymbol{r}_2, \ldots, \boldsymbol{r}_N)$, $R_M = R' = (\boldsymbol{r}'_1, \boldsymbol{r}'_2, \ldots, \boldsymbol{r}'_N)$. In the limit that the *timestep* $\tau = \beta/M \to 0$ the action S has the following simple "primitive approximation" form [19]

$$S(R_0, R_1, R_2, \ldots, R_M) = \sum_{i=1}^{M} \left(\sum_{k=1}^{N} \frac{(\boldsymbol{r}_{k,i} - \boldsymbol{r}_{k,i-1})^2}{4\lambda\tau} + \tau \sum_{k<l} [\phi_{\rm AQ}(r_{kl,i}) + \phi_{\rm HS}(r_{kl,i})] \right) + \frac{dNM}{2} \ln(4\pi\lambda\tau), \tag{3.2}$$

where $r_{kl,i} = |\boldsymbol{r}_{k,i} - \boldsymbol{r}_{l,i}|$ and in $\boldsymbol{r}_{i,j}$ the first index i is a particle label and the second index j is a bead label. We then measure an observable $\mathscr{O}$ through the following trace

$$\langle \mathscr{O} \rangle = \frac{1}{N!} \sum_{\mathscr{P}} \int dR\, \langle R|\mathscr{O} e^{-\beta H}|\mathscr{P} R\rangle, \tag{3.3}$$

where the sum is over all permutations of particle positions $\mathscr{P}R$. If $\mathscr{O}$ is diagonal in position representation

$$\langle \mathscr{O} \rangle = \frac{1}{N!} \sum_{\mathscr{P}} \int dR\, \mathscr{O}(R) \langle R|e^{-\beta H}|\mathscr{P} R\rangle. \tag{3.4}$$

We perform the dNM multidimensional integral and the permutation sum with the *Metropolis algorithm* [20, 21] [1]. Monte Carlo (Metropolis or Markov Chain) is a random walk through phase space using rejections to achieve detailed balance and thereby sample the density matrix. In particular, for the spatial integral we propose a displacement move of the position of a single timeslice k of a single particle i according to $\boldsymbol{r}_{k,i} \to \boldsymbol{r}_{k,i} + \boldsymbol{\Delta}(\eta - 1/2)$ where η is a uniform pseudo-random number in $[0, 1)$ and $\boldsymbol{\Delta}$ a fixed d-dimensional vector whose magnitude is chosen so to have acceptance ratios close to $1/2$. Whereas, for the permutation sum, we propose a swap move of two randomly chosen particles through the *Lévy construction* of a Brownian bridge (see Section V.G of Ref. [19] and references therein). This particular sampling of the permutations sum will never be able to change the winding number of 3 or more particles [19], so we will not be able to measure the superfluid fraction (see our code listing in the supplementary material).

We will measure the following observables:

i. The thermodynamic estimator [19] for the potential energy is

$$\mathscr{O} = \mathscr{V} = \frac{1}{M} \sum_{i=1}^{M} \sum_{k<l=1}^{N} \Phi(r_{kl,i}), \tag{3.5}$$

where $\Phi = \phi_{\mathrm{AQ}} + \phi_{\mathrm{HS}} = \phi_{\mathrm{AQ}}$ since the overlap of any two particles is forbidden.

ii. The thermodynamic estimator [19] for the kinetic energy is

$$\mathscr{O} = \mathscr{K} = \frac{3N}{2\tau} - \frac{1}{M} \sum_{i=1}^{M} \sum_{k=1}^{N} \frac{(\boldsymbol{r}_{k,i} - \boldsymbol{r}_{k,i-1})^2}{4\lambda\tau^2}. \tag{3.6}$$

So that the the total internal energy $\mathscr{O} = \mathscr{E} = \mathscr{K} + \mathscr{V}$.

iii. The virial estimator [19] for the pressure

$$\mathscr{O} = \mathscr{Z} = \frac{\beta}{3N} \left(2\mathscr{K} - \frac{1}{M} \sum_{i=1}^{M} \sum_{k<l=1}^{N} r_{kl,i} \frac{d\Phi(r_{kl,i})}{dr} \right), \tag{3.7}$$

where $\mathscr{Z}$ is the compressibility factor $\beta p/\rho$ with p the pressure.

Note that in the classical HS fluid the potential energy vanishes identically. Not so in the quantum AQHS fluid where the repulsive spiked AQ effective pair potential will prevent any two HS from touching since the spike will produce a smooth repulsive potential profile in a neighborhood of the pair classical contact $r_{ij} = \sigma^+$ that tends to keep apart the pair of particles: they will never be able to touch each other and will instead slip away one from the other contact. We expect this effect to affect the structure of the fluid, its radial distribution function or its structure factor profiles.

Moreover, in the classical HS fluid the compressibility factor only depends on the density or the packing fraction being *athermal* [23, 24]. Not so in the quantum AQHS fluid where the presence of the effective affine potential makes the product $\beta\Phi$ in the density matrix depend on temperature.

So we already see how the two scenarios, the classical realm and the (affine) quantum realm, present profound differences. In the next section we will present our computer experiment results.

IV. NUMERICAL RESULTS

We chose units such that: $\hbar = k_B = \sigma = 1$. We will work with reduced quantities, like the reduced temperature $T^\star = k_B T$, and the reduced density $\rho^\star = \rho\sigma^3$.

In our simulations we had to keep under control 3 sources of error:

i. approach to the *continuum limit* $M \to \infty$ with T constant, which, of course, can be reached only in a theoretical thinking. Here we will adopt the strategy to present all our results at fixed timestep $\tau = 0.08$;

---

[1] Note that a brute force integration with Monte Carlo is not feasible here because the integrand of Eq. (3.4) is very sharply peaked in many dimensions. By doing a random walk rather than a direct sampling, one stays where the integrand is large. But this advantage is also a curse because it is not obvious whether any given walk will converge to its equilibrium distribution in the time available; this is the ergodic problem. This aspect of simulation is experimental; there are no useful theorems, only lots of controlled tests, the lore of the practitioners, and occasional clean comparisons with experimental data. Other subtleties of these methods are how to pick the initial and boundary conditions, determine error bars on the results, compute long-range potentials quickly, and determine physical properties [22].

ii. approach to the *thermodynamic limit* $N \to \infty$ with ρ constant, which, again, can be reached only in a theoretical thinking. This is known as the *finite size error*. In order to make some progress on a finite computer one usually employs periodic boundary conditions so that the simulation box and its periodic images fill up the whole space. Here we will present all our results at fixed $N = 30$;

iii. the *statistical error* which is inherently present in any Monte Carlo calculation. As the previous two sources of error also this one is unavoidable. We will here adopt the strategy of a faithful estimation (through a careful determination of the autocorrelation time during the simulation evolution) of the statistical error bar on any measure that we give.

In Figure 1 we show snapshots of the simulation box taken at the beginning and at the end of the computer experiment.

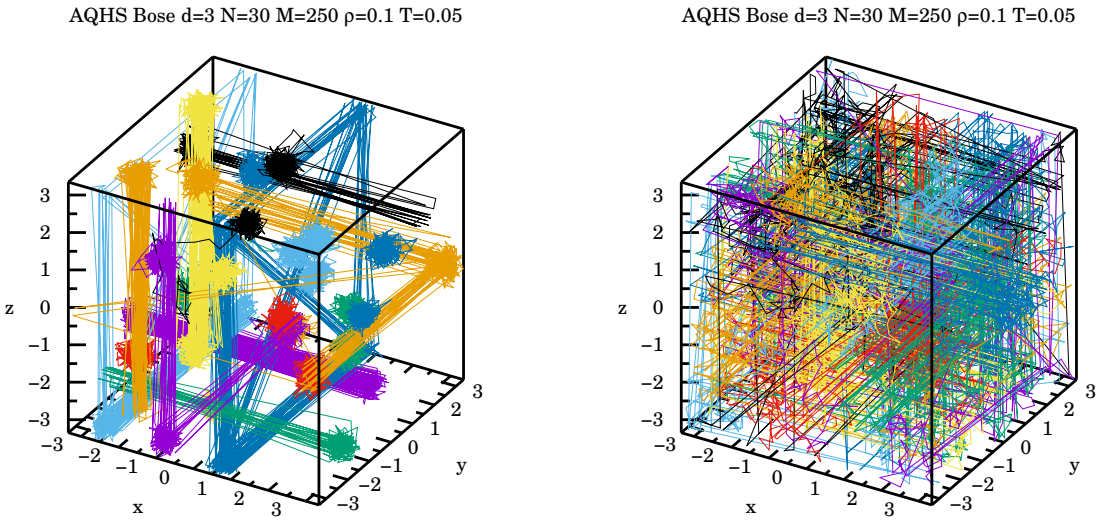

FIG. 1. We show two snapshots of the paths of 30 AQHS made of 250 timeslices each. At a density $\rho^\star = 0.1$ and temperature $T^\star = 0.05$. On the left, at the beginning of the simulation started with the paths at random non-overlapping positions repeated for all the $M = 250$ beads of each of the $N = 30$ paths. On the right, at the end of the simulation when the random walk in the path integral reached equilibrium. During the simulation we measured a kinetic energy per particle $\langle \mathscr{K} \rangle / N k_B T = 39.4(4)$, a potential energy per particle $\langle \mathscr{V} \rangle / N k_B T = 13.41(7)$, and a compressibility factor $\langle \mathscr{Z} \rangle = 172.6(1)$.

In Table I we summarize the numerical results obtained with our PIMC experiment in $d = 3$ with 30 AQHS bosons of unit mass, keeping the timestep $\tau = 0.08$ fixed. During the simulation we only measured thermodynamic quantities like the internal energy and the compressibility factor.

In Figure 2 we plot the results for the compressibility factor presented in Table I and compare them with the Carnahan-Starling (CS) equation of state (eos) [23] for HS in the classical realm. As one can see from the figure at low temperature, when the quantum effects become important, our results indicate a rapid increase of the pressure at all densities. And the monotonous increasing behavior of the pressure as a function of density continues to hold at all temperatures. This increase reflects the tendency of the fluid to crystallize at high densities. We also expect a supersolid behavior in this cases, even if we are not yet ready to measure the superfluid fraction with our present treatment of the permutation sum in Eq. (3.4). More importantly, we see that at high temperature when the path integral reduces to a classical integral nonetheless our results still deviate largely from the CS eos. This should be no surprise since the effective affine potential $\phi_{\rm AQ}$ disappears only in the $\hbar \to 0$ mathematical limit, but not in the $\beta \to 0$ physical regime.

V. CONCLUSIONS

In classical hard-sphere fluids the particles can be variously decorated with adhesion, patchiness, active interaction sites, non-additivity, ..., [25–36] and all these aspects play an important role in modellization in *soft matter physics*.

TABLE I. For a test case of $d = 3$, $N = 30$ boson AQHS particles with $m = 1$ in a cubic periodic cell we measure, with PIMC at fixed $\tau = 0.08$, at various values of the reduced temperature and of the reduced density, the total kinetic energy $\beta\langle\mathscr{K}\rangle$, the total potential energy $\beta\langle\mathscr{V}\rangle$, the total internal energy $\beta\langle\mathscr{E}\rangle$, and the compressibility factor $\langle\mathscr{Z}\rangle$.

M	k_BT	$\rho\sigma^3$	$\langle\mathscr{K}\rangle/Nk_BT$	$-\langle\mathscr{V}\rangle/Nk_BT$	$\langle\mathscr{E}\rangle/Nk_BT$	$\langle\mathscr{Z}\rangle$
250	0.05	0.10	37.0(3)	13.44(4)	23.6(3)	170.94(7)
250	0.05	0.05	17.0(3)	23.62(4)	-6.6(3)	74.5(1)
250	0.05	0.01	2.79(9)	13.38(1)	-10.65(9)	15.73(4)
31	0.40	0.10	4.23(5)	1.60(2)	2.62(5)	21.306(6)
31	0.40	0.05	2.30(5)	2.93(1)	-0.63(5)	9.47(1)
31	0.40	0.01	1.67(3)	1.607(6)	0.06(3)	2.92(1)
12	1.00	0.10	2.65(2)	0.689(6)	1.96(2)	9.013(2)
12	1.00	0.05	1.87(2)	1.122(5)	0.75(2)	4.5049(6)
12	1.00	0.01	1.55(1)	0.586(4)	0.97(1)	1.833(3)
8	1.50	0.10	2.15(2)	0.384(9)	1.77(2)	6.46(1)
8	1.50	0.05	1.73(1)	0.690(6)	1.04(2)	3.440(2)
8	1.50	0.01	1.532(9)	0.366(3)	1.165(9)	1.588(1)

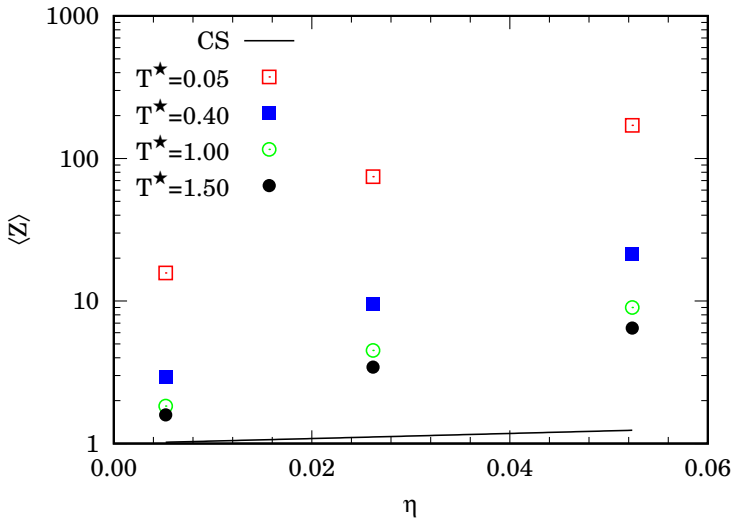

FIG. 2. We show the compressibility factor $\langle\mathscr{Z}\rangle$ as a function of the packing fraction η at various values of reduced temperature, from our numerical results of Table I. For comparison, the Carnahan-Starling (CS) equation of state, $Z = (1+\eta+\eta^2-\eta^3)/(1-\eta)^3$, of classical HS [23] is also shown as a continuous line. The logarithmic scale on the compressibility factor axis is necessary because of the incompressibility nature of the AQHS fluid at low temperature in his extremely quantum regime.

Quantum hard-sphere fluids on the other hand lack, from the very beginning, of a precise definition. This is due to the fact that the momentum operator from the usual canonical-quantization of Dirac ceases to be self-adjoint in presence of forbidden regions or hard boundaries. We here proposed to use the *dilation* operator of affine-quantization [14] in order to reach a well defined statistical mechanics model.

In following this program we soon discovered some profound differences between the hard-sphere fluid in the classical realm and the one in the quantum (affine) realm. In particular the property of the fluid to be athermal in its classical realm and and thermal in its quantum (affine) realm will survive even when taking the high temperature, classical, limit of the quantum (affine) fluid in its path integral formulation. In fact the effective affine potential vanishes only in the $\hbar \to 0$ limit but not in the limit $\beta \to 0$.

We carried out some numerical experiments to measure the thermodynamic properties of this quantum fluid model and drew the equation of state in the pressure-density plane at various fixed values of the temperature. These extend to the quantum realm the ubiquitous Carnahan-Starling [23] equation of state for hard-spheres in the classical realm.

AUTHOR DECLARATIONS

Conflicts of interest

None declared.

Data availability

The data that support the findings of this study are available from the corresponding author upon reasonable request.

Funding

None declared.

[1] J. P. Hansen and I. R. McDonald, *Theory of simple liquids*, 2nd ed. (Academic Press, Amsterdam, 1986) section 3.3.
[2] B. J. Alder and T. E. Wainwright, Phase Transition for a Hard Sphere System, J. Chem. Phys. **27**, 1208 (1957).
[3] B. J. Alder and T. E. Wainwright, Studies in Molecular Dynamics. I. General Method, J. Chem. Phys. **31**, 459 (1959).
[4] W. W. Wood and J. D. Jacobson, Preliminary Results from a Recalculation of the Monte Carlo Equation of State of Hard Spheres, J. Chem. Phys. **27**, 1207 (1957).
[5] H. C. Andersen, J. D. Weeks, and D. Chandler, Relationship between the Hard-Sphere Fluid and Fluids with Realistic Repulsive Forces, Phys. Rev. A **4**, 1597 (1971).
[6] J. D. Weeks, D. Chandler, and H. C. Andersen, Role of Repulsive Forces in Determining the Equilibrium Structure of Simple Liquids, J. Chem. Phys. **54**, 5237 (1971).
[7] H. C. Andersen and D. Chandler, Optimized Cluster Expansions for Classical Fluids. I. General Theory and Variational Formulation of the Mean Spherical Model and Hard Sphere Percus-Yevick Equations, J. Chem. Phys. **57**, 1918 (1972).
[8] E. Thiele, Equation of State for Hard Spheres, J. Chem. Phys. **39**, 474 (1963).
[9] M. S. Wertheim, Exact Solution of the Percus-Yevick Integral Equation for Hard Spheres, Phys. Rev. Lett. **10**, 321 (1963).
[10] M. S. Wertheim, Analytic Solution of the Percus-Yevick Equation, J. Math. Phys. **5**, 643 (1964).
[11] R. J. Baxter, Ornstein-Zernike relation for a disordered fluid, Aust. J. Phys. **21**, 563 (1968).
[12] R. J. Baxter, Ornstein–Zernike Relation and Percus–Yevick Approximation for Fluid Mixtures, J. Chem. Phys. **52**, 4559 (1970).
[13] A. Santos, *A Concise Course on the Theory of Classical Liquids. Basics and Selected Topics*, Lecture Notes in Physics, Vol. 923 (Springer, New York, 2016).
[14] J. R. Klauder and R. Fantoni, The Magnificent Realm of Affine Quantization: valid results for particles, fields, and gravity, Axioms **12**, 911 (2023).
[15] R. Fantoni, *Unifying Classical and Quantum Physics - How classical and quantum physics can pass smoothly back and forth* (Springer, New York, 2025).
[16] J. R. Klauder and R. Fantoni, Thank The Quantum Realm For Nothing Ever Entering Into Black Holes, Int. J. Mod. Phys. A **39**, 2450094 (2024).
[17] R. P. Feynman, The λ-Transition in Liquid Helium, Phys. Rev. **90**, 116 (1953).
[18] R. P. Feynman, A. R. Hibbs, and D. F. Styer, *Quantum Mechanics and Path Integrals*, emended ed. (Dover Publications, 2010) page 292-293.
[19] D. M. Ceperley, Path integrals in the theory of condensed Helium, Rev. Mod. Phys. **67**, 279 (1995).
[20] N. Metropolis, A. W. Rosenbluth, M. N. Rosenbluth, A. M. Teller, and E. Teller, Equation of state calculations by fast computing machines, J. Chem. Phys. **1087**, 21 (1953).
[21] M. H. Kalos and P. A. Whitlock, *Monte Carlo Methods* (John Wiley & Sons Inc., New York, 1986).
[22] M. P. Allen and D. J. Tildesley, *Computer Simulation of Liquids* (Oxford University Press, Oxford, 1987) section 6.2.
[23] N. F. Carnahan and K. E. Starling, Equation of State for Nonattracting Rigid Spheres, J. Chem. Phys. **51**, 635 (1969).
[24] G. A. Mansoori, N. F. Carnahan, K. E. Starling, and T. W. Leland, Equilibrium Thermodynamic Properties of the Mixture of Hard Spheres, J. Chem. Phys. **54**, 1523 (1971).
[25] R. Fantoni and G. Pastore, Computer simulation study of the closure relations in hard sphere fluids, J. Chem. Phys. **120**, 10681 (2004).
[26] R. Fantoni, D. Gazzillo, and A. Giacometti, The thermodynamic instabilities of a binary mixture of sticky hard spheres, Phys. Rev. E **72**, 011503 (2005).

[27] D. Gazzillo, A. Giacometti, R. Fantoni, and P. Sollich, Multicomponent adhesive hard sphere models and short-ranged attractive interactions in colloidal or micellar solutions, Phys. Rev. E **74**, 051407 (2006).
[28] D. Gazzillo, R. Fantoni, and A. Giacometti, Phase behavior of polydisperse sticky hard spheres: analytical solutions and perturbation theory, Mol. Phys. **104**, 3451 (2006).
[29] R. Fantoni, D. Gazzillo, A. Giacometti, and P. Sollich, Phase behavior of weakly polydisperse sticky hard spheres: Perturbation theory for the Percus-Yevick solution, J. Chem. Phys. **125**, 164504 (2006).
[30] R. Fantoni, D. Gazzillo, A. Giacometti, M. A. Miller, and G. Pastore, Patchy sticky hard spheres: analytical study and Monte Carlo simulations, J. Chem. Phys. **127**, 234507 (2007).
[31] R. Fantoni and A. Santos, Nonadditive hard-sphere fuid mixtures. A simple analytical theory, Phys. Rev. E **84**, 041201 (2011).
[32] R. Fantoni and A. Santos, Multicomponent fluid of nonadditive hard spheres near a wall, Phys. Rev. E **87**, 042102 (2013).
[33] R. Fantoni and A. Santos, Depletion force in the infinite-dilution limit in a solvent of nonadditive hard spheres, J. Chem. Phys. **140**, 244513 (2014).
[34] R. Fantoni, Andersen-Weeks-Chandler Perturbation Theory and One-Component Sticky-Hard-Spheres, J. Stat. Phys. **168**, 652 (2017).
[35] R. Fantoni, Effect of quantum dispersion on the radial distribution function of a one-component sticky-hard-sphere fluid, J. Stat. Mech. , 043103 (2018).
[36] R. Fantoni, Monte Carlo simulation of Hard-, Square-Well, and Square-Shoulder Disks in narrow channels, Eur. Phys. J. B **96**, 155 (2023).